DC Link Capacity Enhancement for MMC-based Distribution Link using Dynamic Voltage Operation

van der Sande, Robin; Deshmukh, Rohan; Shekhar, Aditya; Bauer, Pavol

DOI
10.23919/ICPE2023-ECCEAsia54778.2023.10213697

Publication date
2023

Document Version
Final published version

Published in
Proceedings of the 2023 11th International Conference on Power Electronics and ECCE Asia (ICPE 2023 - ECCE Asia)

Citation (APA)
van der Sande, R., Deshmukh, R., Shekhar, A., & Bauer, P. (2023). DC Link Capacity Enhancement for MMC-based Distribution Link using Dynamic Voltage Operation. In *Proceedings of the 2023 11th International Conference on Power Electronics and ECCE Asia (ICPE 2023 - ECCE Asia)* (pp. 636-642). IEEE. https://doi.org/10.23919/ICPE2023-ECCEAsia54778.2023.10213697

DC Link Capacity Enhancement for MMC-based Distribution Link using Dynamic Voltage Operation

Robin van der Sande, Rohan Deshmukh, Aditya Shekhar, and Pavol Bauer
Dept. Electrical Sustainable Energy - Delft University of Technology, The Netherlands

***Abstract*—When operating a modular multilevel converter (MMC), a margin appears between the arm voltage and sum capacitor voltage corresponding to the power dependent ripple. This margin can be used to enhance the DC link voltage and increase the transfer capacity of an MMC-based distribution link while keeping the submodule (SM) stresses fixed. Consequently, this dynamic enhancement in transfer capacity can be achieved with the same submodule switch and capacitor voltage ratings. Using an arm-level averaged simulation model of a 10MW MMC-based MVDC link, the enhancement concept is verified and shown to be beneficial to a practical link application. Besides, a dependency is discovered between the enhancement limit and the grid-injected reactive power, which defines the basis of the proposed control for dynamic enhanced operation.**

***Index Terms*—Power electronic converter, Distribution link, Modular multilevel converter, Power systems**

I. Introduction

Targeting the goal of climate neutrality starts to put a significant strain on the power transmission and distribution systems [1], [2]. With the recent emergence of all-electric houses, heat pump systems, and e-mobility, the localised energy demand has grown significantly. Furthermore, energy consumption has shown an astringent pattern caused by electric vehicle charging [3]. On the other end, renewable generators like wind and photovoltaic possess the downsides of intermittency and unpredictability [2]. Power fluctuations on both the supply and demand side cause curtailment of renewable energy sources and puts stresses on the power distribution infrastructure [4], [5]. All of these contribute toward the more frequent occurrence of congestions in domestic power grids [6], [7]. A commonly proposed solution for grid congestions is to incorporate dc links as a backbone to the existing ac power networks [8]. DC links provide enhanced power flow control, lower operating losses, and improved power transfer capacity over the ac alternative [9], [10]. Implementing dc links can enhance the overall grid stability and improve the utilisation of renewable energy sources by aggregating remote demand-supply imbalances [11], [12]. Also, existing ac links can be repurposed into dc links to enhance the transfer capacity of the given cable [13]. This improved utilisation of the existing grid infrastructure can fulfil the increasing load demand in densely populated areas.

Because of its characteristics, the modular multilevel converter (MMC) can be used to support an exciting medium voltage ac (MVAC) distribution network by incorporating two terminal medium voltage dc (MVDC) distribution links [6]. The MMC is a highly efficient converter which can be used as an interface between an ac grid and a dc bus. It provides promising reliability and fault handling aspects while maintaining a highly scalable design [8]. The MMC-based MVDC distribution link, illustrated in Figure 1, connects two possibly asynchronous ac networks (V_{g1},V_{g2}) via two back-to-back connected MMCs [14]. Normally a MVDC link is operated at a fixed rated dc voltage, set through one of the MMCs. Though as proposed in [15], the distribution link can be operated at an enhanced dc voltage V_d that exceeds the rated value V_{dr} while maintaining the MMC performance under specific operating conditions. This is achieved while preserving both the average stored energy in the MMC and the ac-side harmonic performance. Hence, the MMC can be operated at an enhanced dc voltage while encountering the same submodule (SM) stresses.

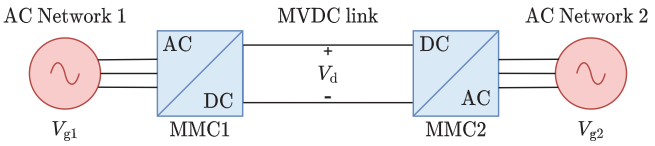

Fig. 1. MVDC distribution link with back-to-back MMCs.

Operating the distribution link at an enhanced dc voltage while maintaining the rated current condition improves the power transfer capacity of the link, e.g. during grid congestions. Consequently, a link capacity enhancement is achieved with the same SM switch and capacitor voltage ratings. Alternatively, for a given operating power, the voltage enhancement can improve the efficiency of the link system by reducing the dc component of the circulating current.

In the present work, the voltage and capacity enhancement concept are explained and verified using a simulation of a 10MW MVDC distribution link. In addition, it elaborates on the challenges encountered when implementing this enhancement in a practical dc distribution link. The rest of the paper is organised as follows: Section II specifies the dc link system parameters and introduces the enhancement concept. Section III, provides various simulation results, indicating the performance of the enhanced link system. Section IV elaborates on the practical implementation concerns. Finally, conclusions are drawn in Section V.

The authors are with the department of Electrical Sustainable Energy in the DCE&S Group at Delft University of Technology. For contact email: R.P.J.vanderSande@tudelft.nl, A.Shekhar@tudelft.nl.
This work is a contribution towards research project: TKI1621/1721 IQ-GRID.

II. Methodology

A. System Description

The simulated 10MW MMC-based MVDC link connects two 10kV ac distribution networks via back-to-back MMCs, forming a symmetrical monopolar configuration. The MMCs are configured along the double-star topology, as shown in Fig. 2 [16]. The six MMC arms are each composed of 9 series connected half-bridge submodules and a 100μH arm inductance. The submodules are constructed using two 3.3kV IGBT switches and a 3.3mF capacitance. During the operation of the distribution link, the link current $i_{\mathrm{d,max}}$ is thermally limited to 585A [9] and the rated dc voltage V_{dr} is set at 17.1kV to ensure compliance with the maximum modulation index as proposed in [17]. Regulating the MMC is a controller which is derived from [18], [19]. The system parameters used during the simulation are summarised in Table I.

TABLE I
MVDC DISTRIBUTION LINK MODEL PARAMETERS

System parameters:	Symbol	Value
Control frequency	f_{c}	10kHz
AC grid:		
Grid frequency	ω_1	314.2 rad/s
Grid voltage L-N (rms)	v_{g}	5.77kV
Grid inductance	L_{g}	287μH
Grid resistance	R_{g}	9mΩ
DC link:		
DC link resistance	R_{l}	0.1Ω
DC link inductance	L_{l}	100μH
Rated DC link voltage	V_{dr}	17.1kV
MMC:		
Rated apparent power	S_{max}	11MVA
Submodule capacitance	C	3.3mF
DC link capacitance	C_{d}	100μF
Number of arm submodules	N	9
Arm inductance	L	4mH
Arm resistance	R	0.1 Ω
Maximum output current	$i_{\mathrm{s,max}}$	907A

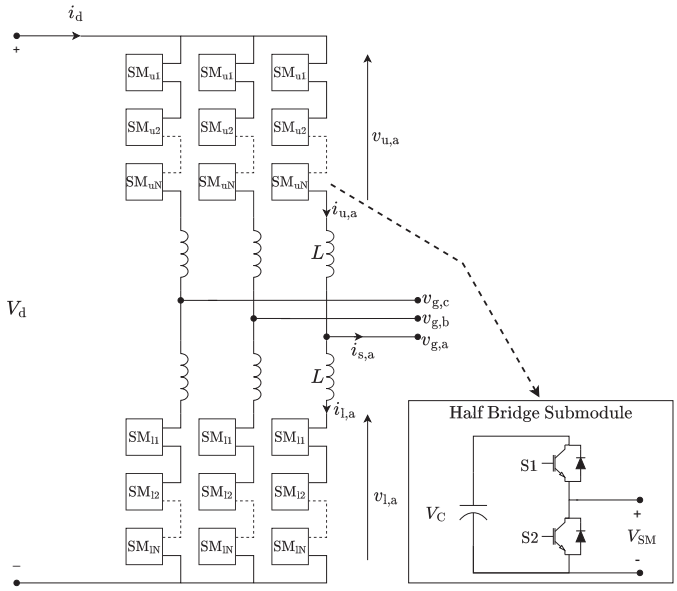

Fig. 2. MMC schematic in double-star configuration.

B. Enhancement Concept

As mentioned in [15], the DC link voltage enhancement considers two crucial quantities of the MMC: the arm voltage $v_{\mathrm{u,l}}$ and the sum capacitor voltage $v^{\Sigma}_{\mathrm{cu,l}}$. The arm voltage is defined as the potential across the arm submodule string and is characterised by (1). $v_{\mathrm{u,l}}$ retains a common-mode phase-leg voltage of $0.5V_{\mathrm{d}}$ and the sinusoidal output voltage of $\hat{v}_s \cos(\omega t)$.

$$v_{\mathrm{u,l}} = v_{\mathrm{c}} \mp v_{\mathrm{s}} = \frac{1}{2}V_{\mathrm{d}} \mp \hat{v}_{\mathrm{s}} \cos(\omega t) \tag{1}$$

The sum capacitor voltage is defined as the sum total of the SM capacitor voltages in the respective arm, and is given by (2). $v^{\Sigma}_{\mathrm{cu,l}}$ is controlled to have an average component V_{d} and has two ripple components caused by the total energy ripple ΔW_{Σ} and imbalance energy ripple ΔW_{Δ} as expressed in (3) and (4), respectively [19], [20]. Note that ΔW_{Σ} and ΔW_{Δ} depend on the operating power of the MMC.

$$v^{\Sigma}_{\mathrm{cu,l}} \approx V_{\mathrm{d}} + \frac{N}{2CV_{\mathrm{d}}}(\Delta W_{\Sigma} + \Delta W_{\Delta}) \tag{2}$$

$$\Delta W_{\Sigma} = -\frac{\hat{V}_{\mathrm{s}}\hat{I}_{\mathrm{s}}}{4\omega_1}\sin(2\omega_1 t - \phi) \tag{3}$$

$$\Delta W_{\Delta} = \frac{V_{\mathrm{d}}\hat{I}_{\mathrm{s}}}{2\omega_1}\sin(\omega_1 t - \phi) - \frac{2\hat{V}_{\mathrm{s}}i_{\mathrm{c}}}{\omega_1}\sin(\omega_1 t) \tag{4}$$

To achieve the link enhancement, the dc voltage V_{d} is operated beyond the nominal value V_{dr}. Though, to preserve the converter performance, both the submodule stresses and the ac side harmonic character must remain equal to the rated condition. Following (1) and (2), the voltage enhancement corresponds to a biasing of the arm voltage $v_{\mathrm{u,l}}$ while maintaining the average sum capacitor voltage $v^{\Sigma}_{\mathrm{cu,l}}$ at V_{dr}. This enhancement concept is illustrated in Fig. 3. The figure contains the sum capacitor voltage and corresponding upper arm voltage for multiple values of the operating dc link voltage. In Fig. 3 V_{dr} is considered as 1 p.u.

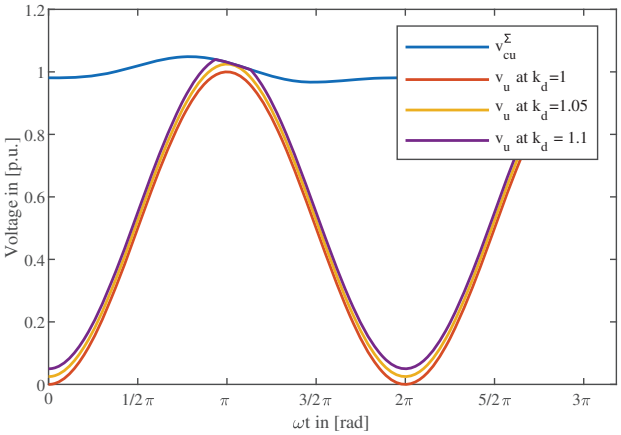

Fig. 3. MMC steady state arm voltages.

It can be concluded from Fig. 3 that the ripple in $v^{\Sigma}_{\text{cu,l}}$, caused by the arm's energy exchange, creates a positive spacing between the $v^{\Sigma}_{\text{cu,l}}$ and $v_{\text{u,l}}$ near $\omega t = \pi$. This ripple margin can be used to bias $v_{\text{u,l}}$, while avoiding an intersection with $v^{\Sigma}_{\text{cu,l}}$. The dc component of $v_{\text{u,l}}$ can thus be increased by an enhancement factor k_d, causing an increase in the dc link voltage to $V_{\text{d}} = k_{\text{d}} V_{\text{dr}}$.

Though, observe from Fig. 3 that the voltage enhancement is limited by the intersection of $v_{\text{u,l}}$ with $v^{\Sigma}_{\text{cu,l}}$. As this intersection of the arm voltage and sum capacitor voltage induces high-frequency arm voltage components, degrading the MMC's output harmonic performance. Eventually, this can lead to stability issues in the converter operation [21].

III. Simulation Results

A. Arm Voltages

To verify the workings of the dc link voltage enhancement, a simulation of the 10MW MMC-based MVDC distribution link is performed. The simulation is based on the arm-level averaged (ALA) model of an MMC, as introduced in [19], [22], [23]. The arm voltage and sum capacitor voltage of the phase a upper arm of MMC1 are simulated. Both MMC1 and MMC2 supply a reactive power Q of 3MVAr to the grid and together provide an active link power P of 10MW. Fig. 4 shows the resulting $v_{\text{u,l}}$ and $v^{\Sigma}_{\text{cu,l}}$ for three values of the enhancement factor $k_{\text{d}} = \{1.0, 1.05, 1.1\}$. It can is concluded that transitioning from no dc voltage enhancement $k_{\text{d}} = 1.0$ to a small enhancement $k_{\text{d}} = 1.05$, the arm voltage is biased but maintains its sinusoidal shape. Meanwhile the sum capacitor voltage is kept at the rated condition. This observation indicates a feasible 5% enhancement of the dc link voltage. Though, at an enhancement of $k_{\text{d}} = 1.1$ the arm voltage intersects the sum capacitor voltage and saturates. This flattening imposes a harmonic distortion in v_{u}, which causes distortion in the sinusoidal output voltage v_{s}. An excessive enhancement thus degrades the output harmonic performance of the MMC. This indicates that the proposed distribution link, operating at the given (P,Q), has a feasible voltage enhancement of $k_{\text{d}} = 1.05$ but fails to comply at $k_{\text{d}} = 1.1$.

B. Enhancement Dependencies

The voltage enhancement utilises the spacing between $v^{\Sigma}_{\text{cu,l}}$ and $v_{\text{u,l}}$ to facilitate the rise in V_{d}. The minimal value of this spacing is defined as the spacing voltage V_{space}, as given by (5). Observe in Fig. 4 that a rise in k_{d} causes a biasing of v_{u}, which in turn results in a reduction of the spacing voltage. Furthermore, notice that if V_{space} becomes zero, harmonic components start to appear in the arm voltage, lowering the MMC ac side performance.

$$V_{\text{space}} = \min_{t \in [0, 2\pi/\omega]} \left(v^{\Sigma}_{\text{cu,l}} - v_{\text{u,l}} \right) \tag{5}$$

To study the impact of the dc link voltage enhancement on V_{space}, a simulation is performed. The result is provided in Fig. 5, which shows the spacing voltage as a function of the enhancement factor k_{d} for different values of Q and a constant value P at 10MW. From Fig. 5 can be concluded that a negative correlation is encountered between the enhancement factor k_{d} and spacing voltage. In accordance with Fig. 4, it is found that the spacing voltage is reduced in order to facilitate the enhancement of the dc side potential. Furthermore, V_{space} is shown to be positively correlated with the operating Q. Which implies that V_{space} can be expanded by operating the converter at a larger reactive power. These two observations combined imply that for a fixed operating spacing voltage, e.g. 430V, an increase in Q enables a rise of the enhancement factor while maintaining the MMC performance. The exact solution of the enhancement factor as a function of reactive power Q is necessary to know, but is not the focus of the current work.

A contrary observation is made from Fig. 6, which shows the spacing voltage as a function of the enhancement factor k_{d} for different values of P and a constant reactive power of 3MVAr. The graph indicates that the spacing voltage is nearly unaffected by the active power passing through the distribution link. This denotes that changes in V_{space} are dominated by changes in k_{d} and not P. For the practical operation of the distribution link, the MMCs are simulated with a modulation index of $m = 0.95$ in accordance with [17]. This caused a preliminary spacing voltage of 390V.

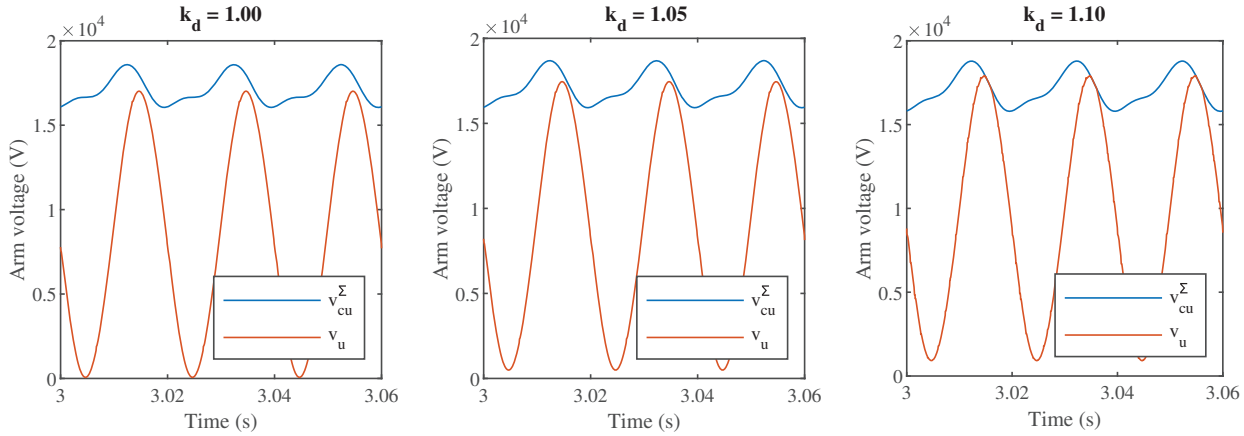

Fig. 4. Simulated MMC arm voltages for different enhancement factors at 3MVAR and 10MW.

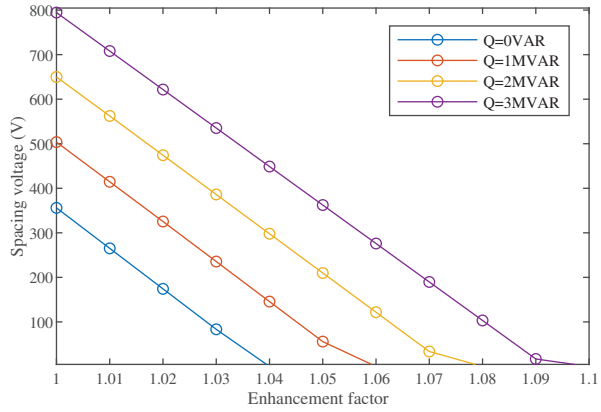

Fig. 5. Spacing voltage at a constant 10MW active power.

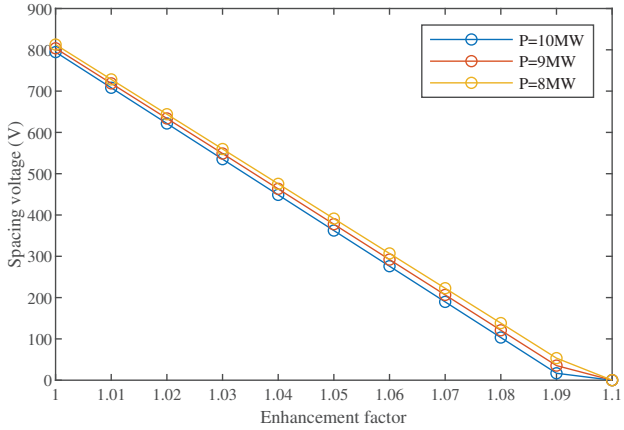

Fig. 6. Spacing voltage at a constant 3MVAR reactive power.

This margin is crucial to handle the total- and imbalance energy ripple in $v^{\Sigma}_{\text{cu,l}}$ for different operating (P,Q). Besides, the spacing is utilised to prevent ac side harmonics injection during system transients. Therefore, a fixed positive V_{space} must be maintained throughout the enhancement to preserve the steady-state and transient ac-side harmonic performance. Using the concept of restricting the operating spacing voltage, the maximum dc voltage enhancement increases with the grid-injected reactive power and remains unaffected by the link's active power.

C. SM Stresses and Harmonic Performance

Another system simulation is performed to verify the preservation of the submodule stresses and ac side harmonic performance under the dc voltage enhancement. Later this is extended to verify the MMC performance under a transfer capacity enhancement of the link. The simulation results are provided in Fig. 7. This figure shows the dc link voltage V_{d}, dc link current I_{d}, active link power P, and the MMC1 spacing voltage, peak SM switch current, sum capacitor voltage all as a function of time. The simulated variables show the response of the dc link system to a 5% voltage enhancement at $t = 3s$ (k_{d} from 1.00 to 1.05) and a 1.5% power enhancement at $t = 4.5s$ (k_{p} from 1.00 to 1.015). During the simulation, MMC1 and MMC2 supply a reactive power Q of 3MVAr to their corresponding ac network, and the link operates at a rated active power of 10MW.

It is observed in Fig. 7 that for $t < 3s$, both the dc link voltage and sum capacitor voltage are in quasi steady state at the rated value of 17.1kV. Meanwhile, the dc link current is constant at 584A to provide the active power transfer of 10MW. Notice that at the rated condition, the peak submodule switch current $\hat{i}_{\text{sw}}$ is 625A. After $t = 3s$, the dc link voltage reference is enhanced by 5% to 18.0kV. Fig. 7 shows the dynamic transition of the V_{d} from its rated value to the enhanced reference. It can be observed that the spacing voltage V_{space} is reduced from 823V to 394V in order to facilitate this voltage enhancement. Because the active link power is maintained, the 5% voltage enhancement causes a 5% reduction in the link current to 556A. This 28A reduction contributes directly to a reduction of the dc circulating current component and lowers the peak submodule switch current from 625A to 615A. Following [12], this leads to an improved efficiency of MMC and corresponding link system. In Fig. 7 can also be observed that the average sum capacitor voltage is controlled constant at the rated value of 17.1kV throughout the enhancement. Note that a downside of the voltage enhancement is the +1.2% increase in capacitor voltage ripple.

The simulation results of Fig. 7 are summarised in Tables II and III, which provide the MMC performance parameters regarding the currents and capacitor voltages, respectively. Table II also provides the total harmonic distortion (THD) of the MMC1's output current i_{s} before and after the voltage enhancement. It is noted that the THDi increases slightly from 0.419% before to 0.422% after the voltage enhancement. So overall the 5% voltage enhancement achieves a system efficiency gain while preserving the submodule switching stresses and maintaining the ac side harmonic performance of the MMC.

TABLE II
MMC PERFORMANCE IN ENHANCED OPERATION: CURRENTS

k_{d}	k_{p}	AC side THD_i (%)		I_{d} (A)	Peak i_{sw} (A)	
1.00	1.00	0.4196	-	583.9	624.76	-
1.05	1.00	0.4226	+0.7%	555.7	615.12	-1.541%
1.05	1.015	0.4111	-2.0%	564.1	623.97	-0.126%
1.10	1.015	0.4606	+9.8%	538.2	616.69	-1.291%

TABLE III
MMC PERFORMANCE IN ENHANCED OPERATION: CAPACITOR VOLTAGE

k_{d}	k_p	Average $v^{\Sigma}_{\text{cu,l}}$ (kV)	Ripple $v^{\Sigma}_{\text{cu,l}}$ (kV)	Δ/μ of $v^{\Sigma}_{\text{cu,l}}$
1.00	1.00	17.12	2.61	15.2%
1.05	1.00	17.12	2.83	16.4%
1.05	1.015	17.12	2.88	16.8%
1.10	1.015	17.14	3.12	18.2%

At $t = 4.5s$, the power reference of the MMCs is enhanced from 10MW to 10.15MW. Fig. 7 shows the dynamic transition of P from the rated to the enhanced value. It can be observed that the spacing voltage and dc link voltage remain nearly

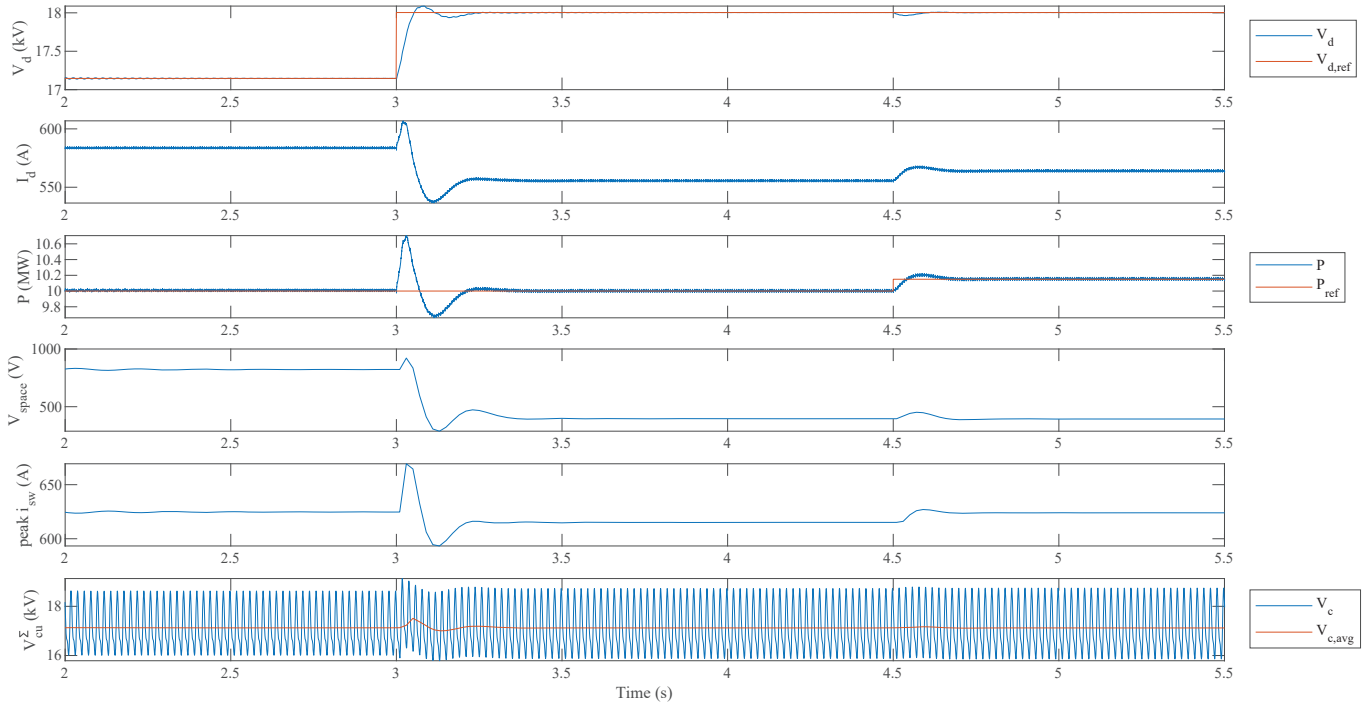

Fig. 7. Performance of MMC-based dc link under voltage- and power enhancement.

unaffected by active power change. Consequently, the link current i_d is enhanced to 564A to enable the active power enhancement. This increase in link current causes a rise in the dc circulating current component, which increases the peak submodule switch current to 624A. The average sum capacitor voltage is again controlled constant at the rated value of 17.1kV. Note that a downside of the power enhancement is the additional +0.4% increase in capacitor voltage ripple. The simulation results of Fig. 7 are again summarised in Tables II and III. From Table II, it is noted that the THDi of MMC1 reduces slightly from 0.419% before to 0.411% after the power enhancement. So overall, the 1.5% active capacity enhancement is achieved while preserving the submodule switching stresses and maintaining the ac side harmonic performance of the MMC.

Additionally, Tables II and III summarise the performance parameters of a 10% voltage enhancement with a 1.5% power enhancement. This excessive enhancement causes the injection of output current harmonics, increasing the THDi by 9.8% compared to the rated operation. This observation is in line with the expectations and verifies the limit to the voltage enhancement. Combined, this set of simulations verifies that the dc link voltage enhancement can accommodate a transfer capacity enhancement in the MVDC distribution link while preserving the SM stresses and the ac side performance.

IV. Implementation Challenges

The previous two sections focus on the link enhancement concept, implying a set of assumptions that simplify the analysis. Though to integrate this concept in a practical MMC-based distribution link, a set of challenges is faced regarding the implementation and operation of the link system. This section elaborates on some of these challenges.

A. Operational Discrepancies

As discovered during the simulations, the set performance constraints limit the rise in the dc voltage. Though, when restricting the spacing voltage, the injection of reactive power extends the voltage enhancement limit. An important assumption made during the simulation is that both MMC1 and MMC2 of the dc link operate at the same reactive power. This operation is illustrated in case 1 of Fig. 8. It was found that case 1 allows for a feasible 5% voltage enhancement.

However, an issue occurs if the MMCs operate at different reactive power references, as shown in case 2 of Fig. 8. Following the result of Fig. 5, it was found that an increase in Q led to an extension of the maximum k_d. This implies that the enhancement limit is bounded by the MMC operating at the lowest reactive power reference. So, in this scenario, MMC1 determines the limit to the voltage and power enhancement.

In case 3 of Fig. 8, both MMCs operate at a reactive power of 3MVAr. Though MMC1 supplies reactive power to the AC network, whereas MMC2 consumes reactive power from the AC network. Following (2), (3), and (4), it is discovered that an MMC consuming reactive power reduces the spacing voltage below the rated condition. This effectively fixes k_d at the lower limit of 1 when the MMC operates at a lagging pf, to ensure compliance with the performance constraints. Combining the three cases leads to the definition of (6), in

which f_{kd} is an empirical function converting Q into the operating enhancement factor.

$$k_{\mathrm{d}} = \max\{1, f_{\mathrm{kd}}(\min\{Q_1, Q_2\})\} \tag{6}$$

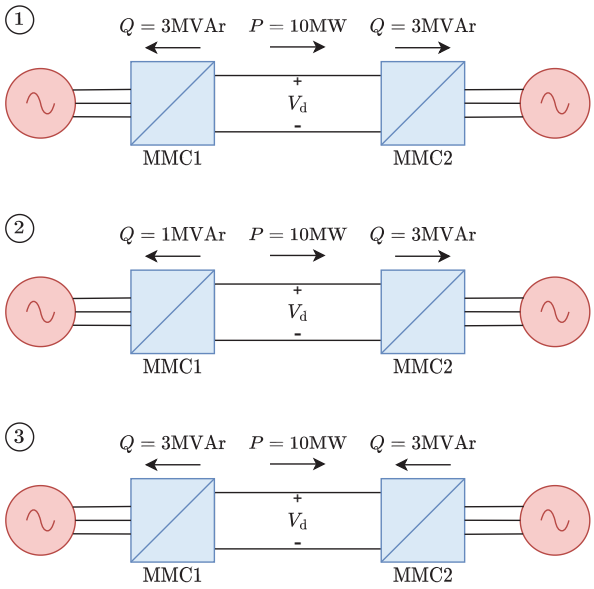

Fig. 8. Operating cases of the dc link system.

B. Design Discrepancies

Another challenge with integrating the enhancement concept in the distribution link system relates to the MMC configuration. Till now, the dc link system was assumed to be in a symmetrical monopolar configuration, where MMC1 and MMC2 have the same structure. Though in practical implementations, the two MMCs might deviate in the number of submodules N and the submodule capacitance C. Notice from (2) that the sum capacitor voltage ripple is directly proportional to N. Similarly, the ripple in $v_{\mathrm{c,u}}^{\Sigma}$ is inversely propositional to C. As this ripple directly affects the spacing voltage, it can be concluded that the MMC with the lowest N to C ratio determines the limit of k_{d} when both MMCs operate at the same Q.

C. Dynamic Operation

Another implementation challenge concerns the dynamic character of the enhanced link system. With practical grid-tied converters, reference changes can occur for both P and Q. Note that the enhancement limit depends on the reactive operating power of the MMC. Therefore any reference change in Q should be done cautiously considering the operated enhancement. For a dynamic implementation of the dc link enhancement, a controller must regulate k_{d}, k_{p} and Q based on an input reference Q^*. As k_{p} is admissible due to voltage enhancement k_{d} and k_{d} is admissible due to the reactive operating power Q, a dependency is imposed. This causes a strict dynamic order for changing k_{d}, k_{p} and Q upon a reference change Q^*. When the MMC operates in an enhanced voltage state, an increase of Q can directly be performed. Once Q has reached its steady state, k_{d} can be increased. Then upon the settling of V_{d}, k_{p} can be enhanced. This process is reflected in (7).

$$\text{Increase in } Q^* : \ [Q \uparrow] \Rightarrow [k_{\mathrm{d}} \uparrow] \Rightarrow [k_{\mathrm{p}} \uparrow] \tag{7}$$

Note that any other order of increasing the three parameters leads to either the injection of harmonic output current components or a significant increase in the peak SM switch current. Alternatively, when the MMC operates in an enhanced voltage state, a decrease of Q can only be done after a significant lowering of V_{d}. Otherwise, harmonic output current components are injected into the ac grid. Though, to allow for the decrease in V_{d}, k_{p} must have been lowered accordingly. Otherwise, the peak SM switch current can exceed the limiting value. This process is reflected in (8).

$$\text{Decrease in } Q^* : \ [k_{\mathrm{p}} \downarrow] \Rightarrow [k_{\mathrm{d}} \downarrow] \Rightarrow [Q \downarrow] \tag{8}$$

The dynamic control procedure alters the operating k_{d}, k_{p} and Q in a stepwise manner. One method to achieve the result is with tuneable time parameters τ_{kd}, τ_{kp} and τ_Q. These reflect the maximum settle time of the corresponding variable to an input reference change. The controller concept is a stable and reliable design philosophy, favouring no constrain violation over dynamic performance.

V. Conclusions and Future Work

When operating an MMC-based dc link, the energy ripple components in the capacitor voltage induce a spacing between the MMC arm voltage and sum capacitor voltage. This margin can be used to enhance the dc link voltage and increase the transfer capacity of the distribution link system. Using a simulation model of a 10MW MVDC link, it is concluded that a 5% dc voltage enhancement can be realised while keeping the SM stresses at the rated condition and preserving the ac-side harmonic performance. This allows the distribution link voltage enhancement to be implemented with the same submodule switch and capacitor voltage ratings. The simulation was then successfully extended to verify the capacity enhancement. It is concluded that a 1.5% transfer capacity enhancement can be achieved in the 10MW dc link when restricting the switching currents to a below-rated condition. Furthermore, it was found from the simulations that the enhancement limit of the link increases with the MMC's grid-injected reactive power and remains unaffected by the link's active power. This observation defined the basis of the implementation challenges and the proposed control strategy for dynamic enhanced operation.

As part of future work, an analytical analysis should be performed to unveil the dependency between the enhancement factor limit and gird-inject reactive power. This notion can then be used to maximise the operating voltage enhancement while preserving MMC performance. In addition, it would form the

basis of the high-level controller, providing a dynamic enhanced operation of the link system. Another aspect of future work relates to the application of the voltage enhancement. The enhancement should be applied to bipolar dc links and multi-terminal MMC-based grids to increase the concept's impact in practical applications.

REFERENCES

[1] H. Schermeyer, M. Studer, M. Ruppert, and W. Fichtner, "Understanding Distribution Grid Congestion Caused by Electricity Generation from Renewables" in International Conference on Smart Energy Research, Essen, DE, 2017, pp. 78-89.

[2] Z. Dalala, M. Al-Omari, M. Al-Addous, M. Bdour, Y. Al-Khasawneh, and M. Alkasrawi, "Increased renewable energy penetration in national electrical grids constraints and solutions" Energy, vol. 246, Feb 2022.

[3] N. Paterakis, M. Gibescu "A methodology to generate power profiles of electric vehicle parking lots under different operational strategies" in Applied Energy, vol. 173, pp. 111-123, Apr 2016.

[4] Y. Gu and L. Xie, "Fast Sensitivity Analysis Approach to Assessing Congestion Induced Wind Curtailment," in IEEE Transactions on Power Systems, vol. 29, no. 1, pp. 101-110, Jan. 2014, doi: 10.1109/TPWRS.2013.2282286.

[5] T. Xu, W. Gao, F. Qian and Y. Li, " The implementation limitation of variable renewable energies and its impacts on the public power grid," in Energy, vol. 239, Part A, Jan. 2022.

[6] S. Khuntia, B. Tuinema, J. Rueda, José, M. van der Meijden, " Time-horizons in the planning and operation of transmission networks: an overview" in IET Generation, Transmission & Distribution, vol. 10, no. 4, pp. 841–848, Oct 2016

[7] R. A. Verzijlbergh, L. J. De Vries and Z. Lukszo, "Renewable Energy Sources and Responsive Demand. Do We Need Congestion Management in the Distribution Grid?," in IEEE Transactions on Power Systems, vol. 29, no. 5, pp. 2119-2128, Sept. 2014, doi: 10.1109/TPWRS.2014.2300941.

[8] N. Ahmed et al., "HVDC SuperGrids with modular multilevel converters — The power transmission backbone of the future," International Multi-Conference on Systems, Signals & Devices, Chemnitz, Germany, 2012, pp. 1-7, doi: 10.1109/SSD.2012.6198119.

[9] A. Shekhar, E. Kontos, L. Ramírez-Elizondo, A. Rodrigo-Mor, and P. Bauer, "Grid capacity and efficiency enhancement by operating medium voltage AC cables as DC links with modular multilevel converters" in Electrical Power and Energy Systems, vol. 93, pp. 479-493, Jun 2017.

[10] Whitepaper, "MVDC PLUS Medium voltage direct current - Managing the future grid," in Siemens AG, 2017.

[11] A. Shekhar, E. Kontos, L. Ramírez-Elizondo and P. Bauer, "AC distribution grid reconfiguration using flexible DC link architecture for increasing power delivery capacity during (n-1) contingency," 2017 IEEE Southern Power Electronics Conference (SPEC), Puerto Varas, Chile, 2017, pp. 1-6, doi: 10.1109/SPEC.2017.8333559.

[12] A. Shekhar, T. B. Soeiro, L. Ramírez-Elizondo and P. Bauer, "Weakly Meshing the Radial Distribution Networks with Power Electronic Based Flexible DC Interlinks," 2019 IEEE Third International Conference on DC Microgrids (ICDCM), Matsue, Japan, 2019, pp. 1-8, doi: 10.1109/ICDCM45535.2019.9232727.

[13] A. Shekhar, L. Ramírez-Elizondo, T. B. Soeiro and P. Bauer, "Boundaries of Operation for Refurbished Parallel AC–DC Reconfigurable Links in Distribution Grids," in IEEE Transactions on Power Delivery, vol. 35, no. 2, pp. 549-559, April 2020, doi: 10.1109/TPWRD.2019.2915198.

[14] M. Saeedifard and R. Iravani, "Dynamic Performance of a Modular Multilevel Back-to-Back HVDC System," in IEEE Transactions on Power Delivery, vol. 25, no. 4, pp. 2903-2912, Oct. 2010.

[15] A. Shekhar, L. Ramírez-Elizondo, Z. Qin, and P. Bauer, "Modular Multilevel Converter Performance with Dynamic MVDC Distribution Link Voltage Rating," in 18TH International Conference on Power Electronics and Motion Control, Budapest, HU, 2018, pp. 1000–1005.

[16] S. Debnath, J. Qin, B. Bahrani, M. Saeedifard and P. Barbosa, "Operation, Control, and Applications of the Modular Multilevel Converter: A Review," in IEEE Transactions on Power Electronics, vol. 30, no. 1, pp. 37-53, Jan. 2015.

[17] Y. Li, X. Shi, B. Liu, F. Wang, and W. Lei, "Maximum modulation index for modular multilevel converter with circulating current control" in IEEE Energy Conversion Congress and Exposition, Pittsburgh, US, 2014, pp. 491–498.

[18] L. Angquist, A. Antonopoulos, D. Siemaszko, K. Ilves, M. Vasiladiotis, and H.-P. Nee, "Open-loop control of modular multilevel converters using estimation of stored energy," IEEE Transactions on Industry Applications,vol. 47, no. 6, pp. 2516–2524, Nov./Dec. 2011.

[19] K. Sharifabadi, L. Harnefors, H. Nee, S. Norrga, and R. Teodorescu, Design, Control, and Application of Modular Multilevel Converters for HVDC Transmission Systems, First edition, Chichester: John Wiley & Sons, 2016.

[20] Q. Song, W. Liu, X. Li, H. Rao, S. Xu and L. Li, "A Steady-State Analysis Method for a Modular Multilevel Converter," in IEEE Transactions on Power Electronics, vol. 28, no. 8, pp. 3702-3713, Aug. 2013.

[21] Z. Liu, K. -J. Li, Z. Guo, J. Wang and J. Qian, "A Comprehensive Study on the Modulation Ratio for Modular Multilevel Converters," in IEEE Transactions on Industry Applications, vol. 58, no. 3, pp. 3205-3216, May-June 2022.

[22] J. Xu, A. M. Gole and C. Zhao, "The Use of Averaged-Value Model of Modular Multilevel Converter in DC Grid," in IEEE Transactions on Power Delivery, vol. 30, pp. 519-528, April 2015.

[23] J. Peralta, H. Saad, S. Dennetiere, J. Mahseredjian and S. Nguefeu, "Detailed and averaged models for a 401-level MMC-HVDC system," in IEEE Power & Energy Society General Meeting, 2013, pp. 1501-1508.